Interactive effect of leaf age and ozone on mesophyll conductance in Siebold's beech

Yasutomo Hoshika[1*], Matthew Haworth[2], Makoto Watanabe[3] and Takayoshi Koike[4]

[1]Institute of Research on Terrestrial Ecosystems (IRET), National Research Council of Italy (CNR), Via Madonna del Piano, I-50019 Sesto Fiorentino, Italy

[2]Institute of Sustainable Plant Protection (IPSP), National Research Council of Italy (CNR), Via Madonna del Piano, I-50019 Sesto Fiorentino, Italy

[3]Institute of Agriculture, Tokyo University of Agriculture and Technology, Fuchu 183-8509, Japan

[4]Research Faculty of Agriculture, Hokkaido University, Sapporo 060-8689, Japan

Correspondence

*Corresponding author,

e-mail: yasutomo.hoshika@cnr.it

Mesophyll conductance (G_m) is one of the most important factors determining photosynthesis. Tropospheric ozone (O_3) is known to accelerate leaf senescence and causes a decline of photosynthetic activity in leaves. However, the effects of age-related variation of O_3 on G_m have not been well investigated, and we, therefore, analysed leaf gas exchange data in a free-air O_3 exposure experiment on Siebold's beech with two levels (ambient and elevated O_3: 28 and 62 nmol mol^{-1} as daylight average, respectively). In addition, we examined whether O_3-induced changes on leaf morphology (leaf mass per area, leaf density and leaf thickness)

may affect CO_2 diffusion inside leaves. We found that O_3 damaged the photosynthetic biochemistry progressively during the growing season. The G_m was associated with a reduced photosynthesis in O_3-fumigated Siebold's beech in August. The O_3-induced reduction of G_m was negatively correlated with leaf density, which was increased by elevated O_3, suggesting that the reduction of G_m was accompanied by changes in the physical structure of mesophyll cells. On the other hand, in October, the O_3-induced decrease of G_m was diminished because G_m decreased due to leaf senescence regardless of O_3 treatment. The reduction of photosynthesis in senescent leaves after O_3 exposure was mainly due to a decrease of maximum carboxylation rate (V_{cmax}) and/or maximum electron transport rate (J_{max}) rather than diffusive limitations to CO_2 transport such as G_m. A leaf age×O_3 interaction of photosynthetic response will be a key for modelling photosynthesis in O_3-polluted environments.

Abbreviations

C_c	CO_2 concentration inside the chloroplast envelope (μmol mol^{-1})
C_i	Sub-stomatal CO_2 concentration (μmol mol^{-1})
ETR	Rate of electron transport (μmol m^{-2} s^{-1})
Φ	Initial slope of photosynthetic light response curve (mol mol^{-1})
Φ_{CO2}	Quantum efficiency of carbon gain (dimensionless)
ΦPSII	Quantum yield of PSII in the light (dimensionless)
Γ	Light compensation point (μmol mol^{-1})
Γ*	CO_2 compensation point to photorespiration (μmol mol^{-1})
G_m	Mesophyll conductance to CO_2 (mol m^{-2} s^{-1} bar^{-1})
G_{sCO2}	Stomatal conductance for CO_2 (mol m^{-2} s^{-1})
G_{sH2O}	Stomatal conductance for water vapour (mol m^{-2} s^{-1})

53	G_{totCO2}	Total conductance to CO_2 (mol m^{-2} s^{-1})
54	J_{max}	Maximum rate of electron transport required for RuBP regeneration (μmol
55	m^{-2} s^{-1})	
56	l_b	Relative biochemical limitation to photosynthesis (%)
57	LD	Leaf density (g cm^{-3})
58	l_b	Relative mesophyll conductance limitation to photosynthesis (%)
59	LMA	Leaf mass per area (g cm^{-2})
60	l_b	Relative stomatal limitation to photosynthesis (%)
61	LT	Leaf thickness (mm)
62	P_N	Net photosynthetic rate (μmol m^{-2} s^{-1})
63	P_{Nsat}	Light-saturated net photosynthetic rate (μmol m^{-2} s^{-1})
64	R_d	Respiration in the light (μmol m^{-2} s^{-1})
65	R_n	Respiration in the dark (μmol m^{-2} s^{-1})
66	R_{PR}	Photorespiration (μmol m^{-2} s^{-1})
67	V_{cmax}	Maximum rate of RuBP carboxylation (μmol m^{-2} s^{-1})
68		
69		
70		
71		
72		
73		
74		
75		
76		
77		
78		

Introduction

Anthropogenic emissions of air pollutants such as nitrogen oxides (NOx) and volatile organic compounds have elevated the ground-level concentration of ozone (O_3) since pre-industrial times (Mills et al. 2018). Ozone is phytotoxic to plants, adversely affecting physiological and biochemical processes contributing to a decline in plant growth (Matyssek et al. 2013, Grulke and Heath 2020).

In cool-temperate forests in Japan, deciduous broadleaved Siebold's beech (*Fagus crenata*) is the dominant tree species (Koike et al. 1998). Previous experimental studies have shown that Siebold's beech is highly sensitive to O_3 (e.g. Yamaguchi et al. 2011, Izuta 2017). Watanabe et al. (2012) estimated that the current concentration of O_3 in Japan may reduce the growth of Siebold's beech from 3.2% to a maximum of 9.7%. This O_3 induced reduction in tree growth is considered to be related to lower photosynthetic activity (Watanabe et al. 2014a). The exact mechanisms underlying the effects of O_3 on photosynthesis are still unclear. However, previous studies have suggested that O_3 causes biochemical limitations associated with reduced ribulose-1,5-bisphosphate carboxylase/oxygenase (Rubisco) activity in leaves (Fiscus et al. 2005, Hoshika et al. 2013, Watanabe et al. 2014a, 2014b, Bagard et al. 2015). The loss of Rubisco activity is commonly inferred from decreases in the maximum rate of carboxylation (V_{cmax}), as indicated by a decrease in the initial slope of a P_N/C_i curve (net photosynthetic rate versus estimated sub-stomatal CO_2 concentration; e.g. Matyssek et al. 2012, Watanabe et al. 2013). Any loss in the biochemical efficiency of CO_2 assimilation induced by O_3 exposure may also be evident in a decline in the maximum rate of electron transport required for ribulose-1,5-bisphosphate (RuBP) regeneration (J_{max}; Hoshika et al. 2013). The traditional calculation of photosynthetic parameters from P_N/C_i curves assumes an infinite mesophyll

conductance to CO_2 (G_m; e.g. Long and Bernacchi 2003). However, G_m may exert similar limits to P_N as stomatal resistance to CO_2 transport (Terashima et al. 1995, Lauteri et al. 2014, Killi and Haworth 2017, Gago et al. 2019, Veromann-Jürgenson et al. 2020). This indicates that previous observations of the O_3-induced reduction of V_{cmax} and J_{max} parameters calculated from P_N/C_i curves assuming infinite G_m incorporate not only biochemical limitations but also the effect of G_m (Warren et al. 2007).

The generation of reactive oxygen species during O_3 exposure could disrupt the physical integrity and biochemistry of mesophyll cells (Kangasjärvi et al. 2005). This would suggest that the exposure to O_3 would impair both the physical and biochemical transport of CO_2 from the sub-stomatal leaf air-space to chloroplasts. In fact, a reduction in G_m was observed in O_3-sensitive snapbean (*Phaseolus vulgaris*) exposed to 60 nmol mol^{-1} O_3, while no effect was observed on the G_m values of resistant varieties (Flowers et al. 2007). Xu et al. (2019) found that the O_3-induced reduction of photosynthesis was mainly due to a decreased G_m in a hybrid poplar clone. In addition, Watanabe et al. (2018a) reported that O_3 exposure reduced G_m in Siebold's beech without any effect on C_c-based V_{cmax}. However, European beech (*F. sylvatica*) grown in an O_3 FACE system showed no effect of a doubling of ambient O_3 concentration on G_m (Warren et al. 2007). Likewise, fumigation of localized areas of Holm oak (*Quercus ilex*) and pubescent oak (*Q. pubescens*) leaves with O_3 between 50 to 350 nmol mol^{-1} did not reduce G_m (Velikova et al. 2005).

Mesophyll conductance is generally lower in leaves with thicker cell walls and greater leaf density (Adachi et al. 2013, Ivanova et al. 2018) that are conditions limiting the diffusion of CO_2 in the leaf liquid phase (Tomás et al. 2013, Onoda et al. 2017). Ozone may affect leaf morphology, which is likely to modify the CO_2

131 diffusion inside leaves (Heath 1994, Moura et al. 2018). The white poplar (*Populus*
132 *alba*) grown in an O_3-enriched atmosphere (150 nmol mol^{-1}) developed thicker and
133 denser leaves than that grown in clean air (Fares et al. 2006). Likewise, leaf density
134 (LD) was increased by O_3 in European silver birch (*Betula pendula*; Oksanen 2005)
135 and European beech (Bussotti et al. 2005). In contrast, the leaves of Pima cotton
136 (*Gossypium barbadense*) formed in O_3-enriched air showed lower mesophyll
137 density (Grantz and Shrestha 2006), probably due to damage and disruption of the
138 mesophyll cells (Günthardt-Goerg et al. 1993). Watanabe et al. (2018a) did not find
139 any effect of O_3 on leaf morphology in Siebold's beech, although plants were
140 exposed to relatively low O_3 concentrations (29 to 47 nmol mol^{-1} as daylight
141 average). The density of cells in the mesophyll layer is closely related to leaf mass
142 per area (LMA; Haworth and Raschi 2014). Meta-analysis suggests that the effect
143 of O_3 on LMA is not pronounced or uni-directional (Poorter et al. 2009), raising
144 the likelihood that O_3 effects on leaf structure depend on species or varieties
145 (Pääkkönen et al. 1995).

146 Previous works have shown that G_m is variable with leaf age (Loreto et al. 1994,
147 Niinemets et al. 2009, Tosens et al. 2012, Marino et al. 2020). After the onset of
148 leaf senescence, G_m reduced due to age-dependent variation of leaf structure and
149 physiological activity (Niinemets et al. 2009). It is known that leaf senescence is
150 accelerated by O_3 (Grulke and Heath 2020). As a matter of fact, O_3-induced
151 structural changes in chloroplasts appear to be similar to those during autumn
152 senescence (e.g. Vollenweider et al. 2019), which may be associated with a reduced
153 mesophyll CO_2 diffusion. The question was therefore raised if O_3 and leaf age
154 could interactively affect G_m, but the age-related change of O_3 effect on G_m has
155 not been addressed in previous studies.

156 To examine a leaf age×O_3 interaction on G_m, we measured leaf gas exchange

three times (June, August, October) in a free-air O_3 exposure experiment on Siebold's beech. The aim of the present study was to: (1) characterise the effect of O_3 fumigation on diffusive resistances to P_N, in particular the impact on G_m values derived from the variable J method (Harley et al. 1992, Loreto et al. 1992), while comparing with those derived from the P_N/C_i curve fitting approach (Ethier and Livingston 2004); (2) assess the impact of O_3 exposure on the efficiency of photosynthetic light capture; and (3) analyse the interaction between O_3 fumigation and leaf morphology (LMA, LD and leaf thickness), and the impact upon photosynthetic physiology throughout the growing season.

Materials and Methods

Experimental site and plant material

Measurements were conducted at a free-air O_3 exposure experiment facility located in the Sapporo Experimental Forest, Hokkaido University, in northern Japan (43°04' N, 141°20' E, 15 m a.s.l., mean annual temperature: 8.9˚C, mean total annual precipitation: 1107 mm, the snow-free period was late April to mid-November). The details of the system are described in Watanabe et al. (2013). The soil is a brown forest soil (Dystric Cambisols). Two plots were established, one for ambient O_3 (AA) and the other for elevated O_3 (eO_3). The size of each plot was 5.5 m × 7.2 m. The distance between the O_3-enhanced plot and the ambient plot was about 20 m, which was enough distance for the O_3-enriched air not to affect the AA plot (Watanabe et al. 2013). Ten seedlings of two-year-old Siebold's beech (*Fagus crenata*) were obtained from a nearby nursery and planted in each plot in May 2003 and then grown under ambient conditions from 2003 to 2010. The plants were ten years old and well-established when fumigation with O_3 began in 2011. The 11-year-old Siebold's beech saplings analysed in this study were around 3.4 m in height in 2012. We confirmed that photosynthetic parameters, plant height and diameter were not different between treatments before O_3 exposure (in July 2011, data not shown). The target O_3 concentration was 60 nmol mol^{-1} during daylight hours. The enhanced O_3 treatment was employed during daylight hours to

187 ten Siebold's beech saplings from August to November in 2011, and from May to
188 November in 2012. Ozone concentrations at canopy height were recorded
189 continuously by an O_3 monitor (Mod. 202, 2B Technologies). The daytime hourly
190 mean of O_3 concentration in AA and eO_3 were 28 nmol mol^{-1} and 62 nmol mol^{-1},
191 respectively, during the 2012 experimental period. The level of O_3 concentration
192 in eO_3 was equal to the environmental standard value in Japan (= 60 nmol mol^{-1}),
193 and has been frequently observed in many Asian regions including forested areas
194 (Izuta 2017). The soil moisture was measured in the root layer (at depth 20 cm) by
195 10HS sensors equipped with an EM5b data logger (Decagon Devices). The average
196 soil moisture (volumetric soil water content) was 28.1 ± 2.8% during these
197 measurements. These values were equivalent to the field capacity of the soil.
198 Previous studies have established that no reduction in P_N due to soil water content
199 occurred during the growing season for Siebold's beech in this experiment
200 (Hoshika et al. 2012, 2013, Watanabe et al. 2014a).

201

202 **Measurement of leaf gas exchange**

203 Leaf gas exchange was measured in fully expanded leaves exposed to full sun at
204 the top of the canopy (n = 6 trees in each O_3 treatment) using a Li6400 portable
205 infra-red gas analyzer (Li-Cor instruments). Only first flush leaves (flushed in
206 May) were used for these measurements, because the number of second flush leaves
207 was very small (0.16% of the total leaf number taken over all saplings).
208 Measurements were undertaken on 15-16 June, 26-31 August and 9-16 October on
209 days with clear sky between 8:00 and 16:00 h. Conditions within the leaf cuvette
210 were set to maintain a leaf temperature of 25°C and the leaf-to-air vapour pressure
211 deficit (VPD) within a range of 1.0-1.8 kPa. The Li6400 was connected to a 6400-
212 40 leaf chamber fluorimeter cuvette with red and blue LEDs when conducting the
213 P_N – photosynthetic photon flux density (PPFD) response curves. The response of
214 P_N to PPFD was measured at 11 light intensities (1500, 1100, 800, 500, 400, 300,
215 200, 100, 75, 50, 0 μmol m^{-2} s^{-1}). At each stage of the P_N/PPFD curve, P_N, stomatal
216 conductance (G_{sH2O}), and the quantum yield of PSII in the light (ΦPSII) were
217 recorded. The P_N/PPFD response curves were utilised to calculate the light
218 saturated rate of P_N (P_{Nsat}), initial slope of photosynthetic light response curve (Φ),
219 light compensation point (Γ) and the quantum efficiency of carbon gain (Φ_{CO2})
220 following Kaipiainen et al. (2009). The Kok (1948) method was used to estimate

respiration in the light (R_d). The effect of variation in the sub-stomatal concentration of [CO_2] (C_i) on R_d was corrected using the iterative method of Kirschbaum and Farquhar (1987). Respiration in the dark (R_n) was measured by switching off the LED light unit after the Kok protocol, shading the area of the plant being measured and recording the rate of CO_2 efflux from the leaf, after values had remained stable for 5-10 min. Mesophyll conductance was calculated at P_{Nsat} using the variable J method as described by Loreto et al. (1992):

$$G_m = \frac{P_{Nsat}}{C_i - \frac{\Gamma^* \cdot [ETR + 8 \cdot (P_N + R_d)]}{ETR - 4 \cdot (P_N + R_d)}} \quad (1),$$

where the electron transport rate (ETR) is calculated from fluorescence (Genty et al. 1989) as following:

$$ETR = \text{PPFD} \cdot \varphi\text{PSII} \cdot \alpha \cdot \beta \quad (2),$$

where the partitioning factor (β) between photosystems I and II was considered to be 0.5 and leaf absorbance (α= 0.85; Laisk and Loreto 1996). The CO_2 compensation point to photorespiration (Γ*) was calculated using the Rubisco specificity factor of Galmes et al. (2005). Total conductance to CO_2 (G_{totCO2}) was calculated as:

$$G_{totCO2} = [G_{sCO2} \cdot G_m]/[G_{sCO2} + G_m] \quad (3).$$

where G_{sCO2} is the stomatal conductance for CO_2. The concentration of [CO_2] inside the chloroplast envelope (C_c) was calculated using the value of G_m produced by the variable J method as:

$$C_c = C_i - \frac{P_{Nsat}}{G_m} \quad (4).$$

Photorespiration (R_{PR}) was determined following Sharkey (1988):

$$R_{PR} = \frac{P_{Nsat} + R_d}{\frac{C_c}{\Gamma^*} - 1} \quad (5).$$

Hoshika et al. (2013) previously reported the P_N/C_i curves of the Siebold's beech exposed to O_3-FACE, based on the approach by Long and Bernacchi (2003) that assumed infinite G_m. Here the P_N/C_i data were re-analysed using the protocol of Ethier and Livingston (2004) to consider G_m values using the curve-fitting approach. The P_N/C_i curves were obtained by measuring P_N over 12 [CO_2] steps (C_a, 380, 300, 220, 140, 60, 300, 380, 500, 800, 1100, 1400, 1700 μmol mol^{-1}). The response of P_N to C_i was then used to calculate the carboxylation capacity of ribulose-1,5-bisphosphate carboxylase/ oxygenase (Rubisco; V_{cmax}) and the maximum rate of electron transport required for ribulose-1,5-bisphosphate (RuBP) regeneration (J_{max}), assuming that G_m were constant at all [CO_2] steps. All gas exchange data were corrected for leaks from gaskets using an empty cuvette and the entire chamber head was enclosed in a plastic bag to minimise the effect of leak (Flexas et al. 2007).

According to Grassi and Magnani (2005), the relative limitations in P_{Nsat} (stomatal limitation, l_s; mesophyll conductance limitation, l_m; biochemical limitation, l_b) were determined as follows:

$$l_s = \frac{G_{totCO2}/G_{sCO2}\cdot\delta P_{Nsat}/\delta C_c}{G_{totCO2}+\delta P_{Nsat}/\delta C_c} \quad (6),$$

$$l_m = \frac{G_{totCO2}/G_m\cdot\delta P_{Nsat}/\delta C_c}{G_{totCO2}+\delta P_{Nsat}/\delta C_c} \quad (7),$$

$$l_b = \frac{G_{totCO2}}{G_{totCO2}+\delta P_{Nsat}/\delta C_c} \quad (8),$$

where $\delta P_{Nsat}/\delta C_c$ is an initial slope of P_N/C_c curves (C_c: over a range of 0–150 μmol mol^{-1}).

Measurements of leaf traits

After the measurement of gas exchange rate, leaves were collected for the determination of the leaf mass per unit area (LMA), leaf density (LD) and leaf thickness (LT). LT was measured avoiding the mid-vein by using a hand-held micrometer (Digimatic micrometer, Mitsutoyo). The projected area (one side of the leaf) was determined with image-processing software (LIA 32, Nagoya University,

Japan). Leaves were then dried in an oven at 70˚C for 1 week and were then weighed. The LMA was calculated as the ratio of the dry mass to the area of the leaves. The LD was calculated as the leaf dry mass per unit leaf volume.

Data analysis

Statistical analyses were performed using R 3.5.1 (R Core Team 2018). To test the effects of O_3 fumigation treatment and measurement months, a two-way ANOVA was used to assess differences in variance between samples. Linear regression was used to investigate possible relationships between P_N and diffusive limitations to CO_2 transport and leaf traits. For these analyses, we used G_m values derived from variable J method. Principle component analysis (PCA) was used to investigate patterns in the photosynthetic capacity, light harvesting and diffusive components of photosynthesis in Siebold's beech after fumigation with O_3. Results were considered significant at $P<0.05$.

Results

Leaf density is modulated by ozone and season

No significant effects of O_3 or measurement month on LMA and LT were found (Table 1). On the other hand, LD was significantly increased by O_3. In addition, LD increased with season as it was relatively smaller in June (0.45 g cm^{-3} in AA and 0.44 g cm^{-3} in eO_3) compared to in October (0.48 g cm^{-3} in AA and 0.54 g cm^{-3} in eO_3).

Photosynthetic parameters are progressively decreased by ozone

Most photosynthetic parameters of Siebold's beech were significantly affected by O_3 exposure (Fig. 1, Table 2). Ozone decreased P_{Nsat} of Siebold beech trees in

August (−28%) and October (−46%), although P_{Nsat} values in both O_3 treatments were similar in June (−7% in eO_3 compared to in AA; Fig. 1A). Significant increases of R_n were induced by O_3 (+70% in August and +88% in October; Fig. 1B). There were no significant changes in R_{PR} associated with elevated O_3 in either June or August (Fig. 1C). However, O_3 decreased R_{PR} by 56% relative to AA plants in October. Ozone decreased G_{sH2O}, G_m and G_{totCO2}, although significant differences were not observed between the treatments in October (Fig. 1D-F). In addition, the measurements by fluorimeter indicated that the PSII electron transport rate (ETR) and actual quantum efficiencies of PSII (ΦPSII) were significantly decreased by O_3 (Table 2, Fig. 2H,L). The eO_3 treatment significantly reduced P_{Nsat} and values of V_{cmax} and J_{max} from the P_N/C_c curves (Table 2, Fig. S1). A significant increase in the J_{max}/V_{cmax} ratio was found in October due to a larger reduction in V_{cmax} than J_{max} after O_3 exposure. Estimated values of G_m derived from the P_N/C_i response curves approach were matched with those calculated by the variable J method (Fig. S2).

Rates of P_{Nsat} were positively correlated to the measures of CO_2 conductance under AA conditions (Fig. 3A-C). However, in eO_3, P_{Nsat} was not associated with G_{sH2O} (Fig. 3A). In addition, no significant relationship between G_m and G_{sH2O} was found in eO_3 (Fig. 3D).

The light-saturated net photosynthetic rate (P_{Nsat}) and diffusive conductance parameters (G_{sH2O}, G_m and G_{totCO2}) were not correlated with LD under the AA condition (Fig. 4A-D). On the other hand, in eO_3, P_{Nsat}, G_m and G_{totCO2} showed negative relationships with LD (Fig. 4A,C,D), while there was no significant correlation between LD and G_{sH2O} (Fig. 4B). LMA and LT did not correlate to those diffusive conductance parameters in both O_3 treatments (Figs S3 and S4).

Relative limitations to photosynthesis are affected by ozone and season

The relative limitations to photosynthesis (l_s, l_m and l_b) are shown in Table 3. Relative limitation to photosynthesis by stomata (l_s) decreased with season. In particular, in eO_3, the reduction in l_s was remarkable in the end of the growing season (l_s: −39% in August, −54% in October compared to June). On the other hand, the l_b increased over the season, and this was highlighted in eO_3 according to the post-hoc Tukey test. A relative limitation to photosynthesis by mesophyll conductance (l_m) was rather constant among the sampling campaigns (approximately 30 to 40% over the season).

Principal component analysis revealed the interaction of leaf age and ozone on photosynthetic response

Principal component analysis of parameters derived from analyses of the photosynthetic capacity (P_N/C_c curves), light harvesting (P_N/PPFD curves) and diffusive limitations to CO_2 transport (G_{sH2O}, G_m and G_{totCO2}) of Siebold's beech indicated a high degree of overlap in the multi-variate space occupied by AA- and eO_3-fumigated plants when measured in June (Fig. 5; student's t-test of PCA scores: component 1, P=0.215; component 2, P=0.646). However, the measurement month affected variations in component 1 and component 2, while O_3 was a significant factor affecting only component 1 (two-way ANOVA of PCA scores: component 1, O_3: P<0.001, Month: P<0.001, O_3×Month: P=0.002; component 2, O_3: P=0.164, Month: P=0.029, O_3×Month: P=0.059). In fact, eO_3-treated plants did not overlap those treated by AA in August and October. In addition, Siebold's beech measured during October occupied distinct multivariate space in comparison to previous analyses in June and August. In this analysis, component 1 accounts for 49.2% of the variance within the dataset and component 2 accounts for 14.8%

365 of variance.
366
367 **Discussion**

368 **Ozone effects on mesophyll conductance and other photosynthetic parameters**

369 We analysed leaf gas exchange data in Siebold's beech exposed to elevated O_3 to
370 assess whether O_3 affected G_m. We found that O_3 caused a significant reduction of
371 G_m in August accompanied by a reduction of P_{Nsat} (Fig. 3B). On the other hand, no
372 significant relationship between G_{sH2O} and P_{Nsat} was found in eO_3 (Fig. 3A). As a
373 result, G_m could better explain the observed reduction of photosynthetic rate rather
374 than G_{sH2O} in eO_3 (Table 3). In addition, the present study indicates that eO_3 caused
375 a decoupling of G_{sH2O} from G_m (Fig. 3D), although a significant relationship has
376 been previously found between G_{sH2O} and G_m (Lloyd et al. 1992, Lauteri et al.
377 2014). Although stomata generally regulate CO_2 uptake, several studies have
378 shown evidence that chronic O_3 exposure impairs efficient stomatal control of gas
379 exchange (Paoletti 2005, Hoshika et al. 2019, 2020).

380 In the previous report by Hoshika et al. (2013), O_3 was found to decrease C_i-
381 based V_{cmax} of Siebold's beech leaves in August and October based on the
382 calculation from P_N/C_i curves assuming an infinite mesophyll conductance to CO_2
383 (Long and Bernacchi 2003). Such a decrease of C_i-based V_{cmax} is, however,
384 attributed to a decreased G_m or degradation of Rubisco activity (Loreto et al. 1994).
385 In the present study, O_3 decreased G_m in August while C_c-based V_{cmax} was not
386 significantly altered (Fig. 1E, Table 2), which is supported by previous findings in
387 Siebold's beech (Watanabe et al. 2018a). In addition, we found that O_3 exposure
388 decreased C_c-based V_{cmax} and J_{max} in October while no reduction was found in G_{sH2O},
389 G_m and G_{totCO2}. The results suggest that a reduction in G_m may be a primary
390 response in O_3-induced decrease of photosynthesis of Siebold's beech.

391

392 **Leaf age effects on mesophyll conductance and other photosynthetic**
393 **parameters**

394 Mesophyll conductance (G_m) decreased with leaf ageing, in association with a
395 reduction of the leaf photosynthetic rate (Fig. 1A, E). Leaf morphological traits
396 were not significantly correlated with G_m during the ageing process in control
397 condition (AA). This is probably because the change in leaf morphology was small
398 during leaf ageing in AA, although LD statistically significantly increased with
399 season. Tosens et al. (2012) similarly reported the slow increase in LD and LMA
400 with leaf ageing after leaf maturity in *Populus tremula*, while LT remained constant.
401 The observed reduction of G_m in senescent leaves may be attributed to age-
402 dependent alterations such as changes of chloroplasts number and size, the location
403 of chloroplasts, photosynthetic enzyme content, and aquaporin status (Evans and
404 Vellen 1996, Niinemets et al. 2009). In addition to G_m, most of photosynthetic
405 parameters decreased with leaf ageing (Fig. 1, Table 2). Interestingly, the relative
406 contribution to photosynthesis by mesophyll conductance (l_m) was rather constant
407 over the season (Table 3). Additionally, the stomatal limitation to photosynthesis
408 (l_s) decreased with leaf ageing, while the relative biochemical limitation (l_b)
409 increased in the end of the growing season. It is known that stomata in senescent
410 leaves remain open even in low light conditions, called the “dull leaf” phenomenon.
411 They are, therefore, unable to regulate leaf gas exchange efficiently (Terashima,
412 2002). On the other hand, the low biochemical photosynthetic capacity in senescent
413 leaves was due to the decline of leaf nitrogen (Watanabe et al., 2018b), which may
414 further limit photosynthesis in autumn. These results suggest that photosynthesis
415 was primarily determined by diffusive limitations of CO_2 transport during summer
416 in Siebold’s beech, while biochemical limitations were relatively important in

417 senescent leaves in autumn. This seasonal change is consistent with the PCA
418 analysis for photosynthetic characteristics (Fig. 5).
419
420 **Interactive effects of ozone and leaf age on leaf gas exchange**
421 Leaf senescence is often accelerated by O_3 exposure (Grulke and Heath 2020). The
422 effects of O_3 on leaf gas exchange were similar to those of leaf senescence, i.e.
423 significant reductions in the photosynthetic capacity, light harvesting and diffusive
424 components of photosynthesis, but the reduction of photosynthetic capacity was
425 observed earlier in eO_3 than in AA (Fig. 1A-F, Table 2). Mesophyll conductance
426 (G_m) showed a sharp decrease after O_3 exposure in August and no further change
427 in October. Meanwhile, LD increased with leaf age especially at eO_3 (Table 1).
428 Previous studies similarly reported that O_3 altered leaf cell ultrastructure in
429 Siebold's beech (Yonekura et al. 2001) and increased LD in European beech
430 (Bussotti et al. 2005). A larger LD may decrease CO_2 diffusion in the liquid phase
431 and, thus, G_m (Niinemets 2015). As a result, a significant relationship between G_m
432 and LD over the season was found at eO_3 (Fig. 4C), suggesting that the reduction
433 of G_m was accompanied by changes in the physical structure of mesophyll cells. It
434 is known that some leaf structural changes are highlighted only when senescence
435 is accelerated by environmental stress (Vollenweider et al. 2019). In fact, as a leaf
436 age×O_3 interaction, inner cell wall thickening has been observed in aged leaves
437 after O_3 exposure due to progressing cell injury in eO_3 (Günthardt-Goerg and
438 Vollenweider 2007). However, we should note that the correlation between LD and
439 G_m was not strong (R^2 = 0.24). This suggests that there may also be other factors
440 causing a reduced G_m after O_3 exposure. For example, aquaporins are involved in
441 the regulation of G_m (e.g. Hanba et al. 2004) and water across the bundle sheath
442 (Shatil-Cohen et al. 2011). Ozone and the resultant reactive oxygen species (ROS)

443 reach the cell membrane (Vainonen and Kangasjärvi 2015), which may affect G_m
444 through direct effects on aquaporins. In fact, O_3 may decrease leaf hydraulic
445 conductance (Zhang et al. 2018), which is related to vein architecture in
446 association with aquaporins (Scoffoni and Sack 2017). This hypothesis needs to be
447 tested in further studies.

448 Limiting factors for the reduction of P_N after O_3 exposure may vary with leaf
449 age. In fact, diffusive resistances to CO_2 transport were dominant factors for
450 photosynthesis at eO_3 in August, while the reduction of P_N after O_3 exposure in
451 October was mainly due to the co-limitation of V_{cmax} and J_{max} (Table 3). At the
452 same time, O_3 progressively increased the J_{max}/V_{cmax} ratio with leaf age (Table 2).
453 This increase in J_{max}/V_{cmax} ratio suggests that the photosynthetic rate was limited
454 more by Rubisco carbon fixation than RuBP regeneration by electron transport.
455 Such a selective degradation of Rubisco quantity or activity was also observed in
456 a poplar clone exposed to O_3 (e.g. Bagard et al. 2008).

457 Rubisco activity is closely related to the capacity of photorespiration (R_{PR})
458 (Farquhar et al. 1980). In fact, R_{PR} in Siebold's beech was decreased by enhanced
459 O_3 treatments with leaf ageing (Fig. 1C). The reduced R_{PR} is equivalent to reduced
460 photoprotective function that, alongside a lower energy usage for photochemistry,
461 would produce ROS, damaging photosynthetic biochemistry (Kangasjärvi et al.,
462 2005). In addition, the plant photorespiratory system requires the glycine
463 decarboxylase (GDC) reaction cycle in the mitochondria, which requires the
464 oxidized form of nicotinamide adenine dinucleotide (NAD+) and generates NADH
465 (the reduced form of NAD; Obata et al. 2016). This decrease in R_{PR} may result in
466 a reduced NADH/NAD+ ratio stimulating mitochondrial respiration (Dizengremel
467 et al. 2012) as confirmed here in the O_3-induced increase of dark respiration rate
468 (Fig. 1B).

Conclusion

Our results indicate that O_3 damaged photosynthetic mechanisms in Siebold's beech leaves. Mesophyll conductance was associated with a reduced photosynthesis in O_3-fumigated Siebold's beech in August. This O_3-induced reduction of G_m was negatively correlated with leaf density, which was increased by O_3 exposure. This suggests that the reduction of G_m in August was accompanied by changes in the physical structure of mesophyll cells. However, the response of photosynthetic parameters to O_3 was different in the later growing season. In October, the O_3-induced reduction of photosynthesis was mainly due to the co-limitation of V_{cmax} and J_{max} rather than diffusive resistances to CO_2 transport. Mesophyll conductance (G_m) decreased in October due to leaf senescence regardless of O_3 treatments. In consequence, the O_3-induced decrease of G_m was diminished. These results suggest that seasonal changes of the photosynthetic response to O_3 will be a key to modelling photosynthesis in an O_3-polluted environment.

Author contributions

Y.H. conceived the study and methodology, and analysed leaf gas exchange data from the ozone FACE experiment performed by Y.H., M.W. and T.K.; M.H. co-conceived the study and contributed to the analysis of light-response curve. All authors were involved in writing the paper, although Y.H. took a lead role.

Acknowledgement

We are grateful to Mr. Naoki Inada and Mr. Tatsushiro Ueda for technical support. This work was partly supported by the Environment Research and Technology

Development Fund (B-1105) of the Ministry of the Environment, Japan, and by a Grant-in-aid from the Japanese Society for Promotion of Science (Type B 23380078, Young Scientists B 24780239 and ditto B 15K16136) as well as JST, Japan (JPMJSC18HB) to MW and TK. We are also grateful for financial support to the LIFE+ project MOTTLES (LIFE15 ENV/IT/000183) of the European Commission.

Data availability statement

Data sharing is not applicable to this article as all new created data is already contained within this article.

References

Adachi S, Nakae T, Uchida M, Soda K, Takai T, Oi T, Yamamoto T, Ookawa T, Miyake H, Yano M, Hirasawa T (2013). The mesophyll anatomy enhancing CO_2 diffusion is a key trait for improving rice photosynthesis. J Exp Bot 64: 1061-1072

Bagard M, Jolivet Y, Hasenfratz-Sauder M-P, Gérard J, Dizengremel P, Le Thiec D (2015) Ozone exposure and flux-based response functions for photosynthetic traits in wheat, maize and poplar. Environ Pollut 206: 411–420

Bagard M, Le Thiec D, Delacote E, Hasenfratz-Sauder M-P, Banvoy J, Gérard J, Dizengremel P, Jolivet Y (2008) Ozone-induced changes in photosynthesis and photorespiration of hybrid poplar in relation to the developmental stage of the leaves. Physiol Plant 134: 559–574

Bussotti F, Agati G, Desotgiu R, Matteini P, Tani C (2005) Ozone foliar symptoms in woody plant species assessed with ultrastructural and fluorescence analysis.

521 New Phytol 166: 941–955
522 Dizengremel P, Vaultier M-N, Le Thiec D, Cabané M, Bagard M, Gérant D, Gérard
523 J, Allah Dghim A, Richet N, Afif D, Pireaux J-C, Hasenfratz-Sauder M-P, Jolivet
524 Y (2012) Phosphoenolpyruvate is at the crossroads of leaf metabolic responses
525 to ozone stress. New Phytol 195: 512–517
526 Ethier GJ, Livingston NJ (2004) On the need to incorporate sensitivity to CO_2
527 transfer conductance into the Farquhar–von Caemmerer–Berry leaf
528 photosynthesis model. Plant Cell Environ 27: 137–153
529 Evans JR, Vellen L (1996) Wheat cultivars differ in transpiration efficiency and
530 CO_2 diffusion inside their leaves. In: Ishii R, Horie T (ed) Crop research in Asia:
531 Achievements and perspective. Asian Crop Science Association, Tokyo, pp. 326–
532 329
533 Fares S, Barta C, Brilli F, Centritto M, Ederli L, Ferranti F, Pasqualini S, Reale L,
534 Tricoli D, Loreto F (2006) Impact of high ozone on isoprene emission,
535 photosynthesis and histology of developing *Populus alba* leaves directly or
536 indirectly exposed to the pollutant. Physiol Plant 128: 456-465
537 Farquhar GD, von Caemmerer S, Berry JA (1980) A biochemical model of
538 photosynthetic CO_2 assimilation in leaves of C3 species. Planta 149: 78-90
539 Fiscus EL, Booker FL, Burkey KO (2005) Crop responses to ozone: uptake, modes
540 of action, carbon assimilation and partitioning. Plant Cell Environ 28: 997–1011
541 Flexas J, Díaz-Espejo A, Berry JA, Cifre J, Galmés J, Kaldenhoff R, Medrano H,
542 Ribas-Carbó M (2007) Analysis of leakage in IRGA's leaf chambers of open gas
543 exchange systems: quantification and its effects in photosynthesis
544 parameterization. J Exp Bot 58: 1533–1543

545 Flowers MD, Fiscus EL, Burkey KO, Booker FL, Dubois JB (2007) Photosynthesis,
546 chlorophyll fluorescence, and yield of snap bean (*Phaseolus vulgaris* L.)
547 genotypes differing in sensitivity to ozone. Environ Exp Bot, 61: 190-198
548 Gago J, Carriquí M, Nadal M, Clemente-Moreno MJ, Coopman RE, Fernie AR,
549 Flexas J (2019) Photosynthesis optimized across land plant phylogeny. Trends
550 Plant Sci 24: 947-958
551 Galmes J, Flexas J, Keys AJ, Cifre J, Mitchell RAC, Madgwick PJ, Haslam RP,
552 Medrano H, Parry MAJ (2005) Rubisco specificity factor tends to be larger in
553 plant species from drier habitats and in species with persistent leaves. Plant Cell
554 Environ 28: 571-579
555 Genty B, Briantais J-M, Baker NR (1989) The relationship between the quantum
556 yield of photosynthetic electron transport and quenching of chlorophyll
557 fluorescence. Biochimica et Biophysica Acta (BBA)-General Subjects 990: 87–
558 92
559 Grantz DA, Shrestha A (2006) Tropospheric ozone and interspecific competition
560 between Yellow nutsedge and Pima cotton. Crop Sci 46: 1879–1889
561 Grassi G, Magnani F (2005) Stomatal, mesophyll conductance and biochemical
562 limitations to photosynthesis as affected by drought and leaf ontogeny in ash
563 and oak trees. Plant Cell Environ 28: 834–849
564 Grulke NE, Heath RL (2020) Ozone effects on plants in natural ecosystems. Plant
565 Biol 22 (S1): 12–37
566 Günthardt-Goerg MS, Matyssek R, Scheidegger C, Keller T (1993). Differentiation
567 and structural decline in the leaves and bark of birch (*Betula pendula*) under low
568 ozone concentrations. Trees 7: 104-114
569 Hanba YT, Shibasaka M, Hayashi Y, Hayakawa T, Kasamo K, Terashima I,
570 Katsuhara M (2004). Overexpression of the barley aquaporin HvPIP2;1 increases

internal CO_2 conductance and CO_2 assimilation in the leaves of transgenic rice plants. Plant Cell Physiol 45: 521-529

Harley PC, Loreto, F., Dimarco, G., Sharkey, T.D. (1992) Theoretical considerations when estimating the mesophyll conductance to CO_2 flux by analysis of the response of photosynthesis to CO_2. Plant Physiol 98: 1429-1436

Heath RL (1994). Possible mechanisms for the inhibition of photosynthesis by ozone. Photosyn Res 39: 439-451

Harley PC, Loreto, F., Dimarco, G., Sharkey, T.D. (1992) Theoretical considerations when estimating the mesophyll conductance to CO_2 flux by analysis of the response of photosynthesis to CO_2. *Plant Physiol.*, **98**, 1429-1436

Hoshika Y, De Carlo A, Baraldi R, Neri L, Carrari E, Agathokleous E, Zhang L, Fares S, Paoletti E (2019) Ozone-induced impairment of night-time stomatal closure in O_3-sensitive poplar clone is affected by nitrogen but not by phosphorus enrichment. Sci Tot Environ 692: 713-722

Hoshika Y, Fares S, Pellegrini E, Conte A, Paoletti E (2020) Water use strategy affects avoidance of ozone stress by stomatal closure in Mediterranean trees—A modelling analysis. Plant Cell Environ 43: 611-623

Hoshika Y, Watanabe M, Inada N, Koike T (2012) Modeling of stomatal ozone conductance for estimating ozone uptake of *Fagus crenata* under experimentally enhanced free-air ozone exposure. Wat Air Soil Pollut 223: 3893-3901

Hoshika Y, Watanabe M, Inada N, Koike T (2013) Model-based analysis of avoidance of ozone stress by stomatal closure in Siebold's beech (*Fagus crenata*). Ann Bot 112: 1149-1158

Ivanova LA, Yudina PK, Ronzhina DA, Ivanov LA, Hölzel N (2018) Quantitative mesophyll parameters rather than whole-leaf traits predict response of C_3 steppe plants to aridity. New Phytol 217: 558-570

597 Izuta T (2017) Air Pollution Impacts on Plants in East Asia. Springer-Verlag, Tokyo
598 Kaipiainen EL (2009) Parameters of photosynthesis light curve in *Salix dasyclados*
599 and their changes during the growth season. Russian J Plant Physiol 56: 445-453
600 Kangasjärvi J, Jaspers P, Kollist H (2005) Signalling and cell death in ozone-
601 exposed plants. Plant Cell Environ 28: 1021-1036
602 Killi D, Haworth M (2017) Diffusive and metabolic constraints to photosynthesis
603 in Quinoa during drought and salt stress. Plants 6: 49
604 Kirschbaum MU, Farquhar GD (1987) Investigation of the CO_2 dependence of
605 quantum yield and respiration in *Eucalyptus pauciflora*. Plant Physiol 83: 1032-
606 1036
607 Koike T, Kato S, Shimamoto Y, Kitamura K, Kawano S, Ueda K, Mikami T (1998)
608 Mitochondrial DNA variation follows a geographic pattern in Japanese beech
609 species. Botanica Acta 111: 87-92
610 Kok B (1948) A critical consideration of the quantum yield of Chlorella
611 photosynthesis. Enzymologia 13: 1–56
612 Laisk A, Loreto F (1996) Determining photosynthetic parameters from leaf CO_2
613 exchange and chlorophyll fluorescence: Rubisco specificity factor, dark
614 respiration in the light, excitation distribution between photosystems,
615 alternative electron transport rate and mesophyll diffusion resistance. Plant
616 Physiol 110: 903–912
617 Lauteri M, Haworth M, Serraj R, Monteverdi MC, Centritto M (2014)
618 Photosynthetic diffusional constraints affect yield in drought stressed rice
619 cultivars during flowering. Plos one 9: e109054
620 Long SP, Bernacchi CJ (2003) Gas exchange measurements, what can they tell us
621 about the underlying limitations to photosynthesis? Procedures and sources of
622 error. J Exp Bot 54: 2393-2401

623 Loreto F, Di Marco G, Tricoli D, Sharkey TD (1994) Measurements of mesophyll
624 conductance, photosynthetic electron transport and alternative electron sinks of
625 field grown wheat leaves. Photosyn Res 41: 397–403
626 Loreto F, Harley PC, Di Marco G, Sharkey TD (1992) Estimation of mesophyll
627 conductance to CO_2 flux by three different methods. Plant Physiol 98: 1437–
628 1443
629 Marino G, Haworth M, Scartazza A, Tognetti R, Centritto M (2020) A Comparison
630 of the variable J and carbon-isotopic composition of sugars methods to assess
631 mesophyll conductance from the leaf to the canopy scale in drought-stressed
632 cherry. Int J Mol Sci 21(4): 1222
633 Matyssek R, Schnyder H, Oßwald W, Ernst D, Munch JC, Pretzsch H (2012) Growth
634 and Defence in Plants; Resource Allocation at Multiple Scales. Springer V.,
635 Heidelberg, 470 pp
636 Matyssek R, Clarke N, Cudlin P, Mikkelsen TN, Tuovinen JP, Wieser G, Paoletti E
637 (2013) Climate change, air pollution and global challenges: understanding and
638 perspectives from forest research. Developments in Environmental Science 13.
639 Elsevier, Amsterdam, 622 pp
640 Mills G, Pleijel H, Malley CS, Sinha B, Cooper O, Schultz M, Neufeld HS, Simpson
641 D, Sharps K, Feng Z, Gerosa G, Harmens H, Kobayashi K, Saxena P, Paoletti E,
642 Sinha V, Xu X (2018) Tropospheric Ozone Assessment Report: Present day
643 tropospheric ozone distribution and trends relevant to vegetation. Elementa
644 Science of the Anthropocene 6(1): 47
645 Moura BB, Alves ES, Marabesi MA, de Souza SR, Schaub M, Vollenweider P
646 (2018). Ozone affects leaf physiology and causes injury to foliage of native tree
647 species from the tropical Atlantic Forest of southern Brazil. Sci Tot Environ 610-
648 611: 912-925

649 Niinemets Ü (2015) Is there a species spectrum within the world-wide leaf
650 economics spectrum? Major variations in leaf functional traits in the
651 Mediterranean sclerophyll *Quercus ilex*. New Phytol 205: 79–96
652 Niinemets Ü, Díaz-Espejo A, Flexas J, Galmés J, Warren CR (2009) Role of
653 mesophyll diffusion conductance in constraining potential photosynthetic
654 productivity in the field. J Exp Bot 60: 2249-2270
655 Obata T, Florian A, Timm S, Bauwe H, Fernie AR (2016). On the metabolic
656 interactions of (photo)respiration. J Exp Bot 67: 3003-3014
657 Oksanen E (2005). Northern conditions enhance the susceptibility of birch (*Betula*
658 *pendula* Roth) to oxidative stress caused by ozone. In: Omasa K, Nouchi I, De
659 Kok LJ (ed) Plant responses to air pollution and global change. Springer-Verlag,
660 Tokyo, pp 29–35
661 Onoda Y, Wright IJ, Evans JR, Hikosaka K, Kitajima K, Niinemets Ü, Poorter H,
662 Tosens T, Westoby M (2017) Physiological and structural tradeoffs underlying
663 the leaf economics spectrum. New Phytol 214: 1447–1463
664 Paoletti E (2005) Ozone slows stomatal response to light and leaf wounding in a
665 Mediterranean evergreen broadleaf, *Arbutus unedo*. Environ Pollut 134: 439–
666 445
667 Pääkkönen E, Holopainen T, Kärenlampi L (1995). Ageing-related anatomical and
668 ultrastructural changes in leaves of birch (*Betula pendula* Roth.) clones as
669 affected by low ozone exposure. Ann Bot 75: 285-294
670 Poorter H, Niinemets Ü, Poorter I, Wright IJ, Villar R (2009). Causes and
671 consequences of variation in leaf mass per area (LMA): a meta-analysis. New
672 Phytol 182: 565-588
673 R Core Team (2018) R: A language and environment for statistical computing.
674 Vienna, Austria: R Foundation for Statistical Computing. Retrieved from

https://www.R-project.org/

Scoffoni C, Sack L (2017) The causes and consequences of leaf hydraulic decline with dehydration. J Exp Bot 68: 4479-4496

Sharkey TD (1988) Estimating the rate of photorespiration in leaves. Physiol Plant 73: 147– 152

Shatil-Cohen A, Attia Z, Moshelion M (2011). Bundle-sheath cell regulation of xylem-mesophyll water transport via aquaporins under drought stress: a target of xylem-borne ABA? The Plant J 67: 72-80

Terashima I. (2002) Photosynthesis at leaf and individual level. In: Sato K (ed) Photosynthesis. Asakura, Tokyo, pp. 125-149 (in Japanese)

Terashima I, Ishibashi M, Ono K, Hikosaka K (1995). Three resistances to CO_2 diffusion: leaf-surface water, intercellular spaces and mesophyll cells. In: Mathis P (ed) Photosynthesis: from light to biosphere, Vol. V. Kluwer Academic Publishers, Dordrecht, pp. 537–542

Tomás M, Flexas J, Copolovici L, Galmés J, Hallik L, Medrano H, Ribas-Carbó M, Tosens T, Vislap V, Niinemets Ü (2013). Importance of leaf anatomy in determining mesophyll diffusion conductance to CO_2 across species: quantitative limitations and scaling up by models. J Exp Bot 64: 2269-2281

Tosens T, Niinemets Ü, Vislap V, Eichelmann H, Díez PC (2012) Developmental changes in mesophyll diffusion conductance and photosynthetic capacity under different light and water availabilities in *Populus tremula*: how structure constrains function. Plant Cell Environ 35: 839–856

Vainonen JP, Kangasjärvi J (2015) Plant signaling in acute ozone exposure. Plant Cell Environ 38: 240-252

Velikova V, Tsonev T, Pinelli P, Alessio GA, Loreto F (2005) Localized ozone fumigation system for studying ozone effects on photosynthesis, respiration,

electron transport rate and isoprene emission in field-grown Mediterranean oak species. Tree Physiol 25: 1523-1532

Veromann-Jürgenson L-L, Brodribb TJ, Niinemets Ü, Tosens T (2020) Pivotal role of mesophyll conductance in shaping photosynthetic performance across 67 structurally diverse gymnosperm species. Int J Plant Sci 181: 116-128

Watanabe M, Hoshika Y, Inada N, Koike T (2014a) Canopy carbon budget of Siebold's beech (*Fagus crenata*) sapling under free air ozone exposure. Environ Pollut 184: 682-689

Watanabe M, Hoshika Y, Inada N, Koike T (2018b) Photosynthetic activity in relation to a gradient of leaf nitrogen content within a canopy of Siebold's beech and Japanese oak saplings under elevated ozone. Sci Tot Environ 636: 1455-1462

Watanabe M, Hoshika Y, Inada N, Wang X, Mao Q, Koike T (2013) Photosynthetic traits of Siebold's beech and oak saplings grown under free air ozone exposure. Environ Pollut 174: 50-56

Watanabe M, Hoshika Y, Koike T (2014b) Photosynthetic responses of Monarch birch seedlings to differing timings of free air ozone fumigation. J Plant Res 127: 339-345

Watanabe M, Komimaki Y, Mori M, Okabe S, Arakawa I, Kinose Y, Izuta T (2018a) Mesophyll conductance to CO_2 in leaves of Siebold's beech (*Fagus crenata*) seedlings under elevated ozone. J Plant Res 131: 907-914

Watanabe M, Yamaguchi M, Matsumura H, Kohno Y, Izuta T (2012) Risk assessment of ozone impact on *Fagus crenata* in Japan: consideration of atmospheric nitrogen deposition. Europ J For Res 131: 475-484

725 Warren CR, Löw M, Matyssek R, Tausz M (2007) Internal conductance to CO_2
726 transfer of adult *Fagus sylvatica*: Variation between sun and shade leaves and
727 due to free-air ozone fumigation. Environ Exp Bot 59: 130-138
728 Xu Y, Feng Z, Shang B, Dai L, Uddling J, Tarvainen L (2019) Mesophyll
729 conductance limitation of photosynthesis in poplar under elevated ozone. Sci Tot
730 Environ 657: 136-145
731 Yamaguchi M, Watanabe M, Matsumura H, Kohno Y, Izuta T (2011) Experimental
732 studies on the effects of ozone on growth and photosynthetic activity of Japanese
733 forest tree species. Asian J Atmos Environ 5: 65-78, doi:
734 10.5572/ajae.2011.5.2.065
735 Yonekura T, Honda Y, Oksanen E, Yoshidome M, Watanabe M, Funada R, Koike T,
736 Izuta T (2001) The influences of ozone and soil water stress, singly and in
737 combination, on leaf gas exchange rates, leaf ultrastructural characteristics and
738 annual ring width of *Fagus crenata* seedlings. J Jpn Soc Atmos Environ 36: 333-
739 351
740 Zhang WW, Wang M, Wang AY, Yin XH, Feng ZZ, Hao GY (2018) Elevated ozone
741 concentration decreases whole-plant hydraulic conductance and disturbs water
742 use regulation in soybean plants. Physiol Plant 163: 183-195
743

744 **Supporting information**
745 Additional Supporting Information may be found in the online version of this
746 article:
747 **Fig. S1.** Responses of net photosynthetic rate (P_N) to the sub-stomatal
748 concentration of CO_2 (C_i) or the concentration of CO_2 inside the chloroplast
749 envelope (C_c).
750 **Fig. S2.** Relationship between mesophyll conductance (G_m) values derived from
751 the variable J method and those derived from the P_N/C_i curve fitting method.
752 **Fig. S3.** Relationships between leaf gas exchange parameters and leaf mass per

753 area (LMA) of Siebold's beech saplings.
754 **Fig. S4.** Relationships between leaf gas exchange parameters and leaf thickness
755 (LT) of Siebold's beech saplings.
756
757
758 **Figure legends**
759 **Figure 1.** Photosynthetic parameters of Siebold's beech grown under ambient (AA)
760 and elevated O_3 (eO_3). (A) Light-saturated net photosynthetic rate [P_{Nsat}], (B) dark
761 respiration rate [R_N], (C) photorespiration [R_{PR}], (D) stomatal conductance to water
762 vapor [G_{sH2O}], (E) mesophyll conductance to CO_2 [G_m], (F) total conductance to
763 CO_2 [G_{totCO2}]. Each value is the mean ± standard error (n=6). Two-way ANOVA: *
764 P<0.05, ** P<0.01, *** P<0.001, ns denotes not significant. Different letters show
765 significant differences among treatments (P<0.05, Tukey test).
766 **Figure 2.** Responses of net photosynthetic rate (P_N), stomatal conductance (G_{sH2O}),
767 mesophyll conductance (G_m) and electron transport rate (ETR) to photosynthetic
768 photon flux density (PPFD). The P_N/PPFD curves were obtained by measuring P_N
769 over 11 PPFD steps (1500, 1100, 800, 500, 400, 300, 200, 100, 75, 50, 0 μmol m^{-2}
770 s^{-1}) in Siebold's beech exposed to different O_3 concentrations (ambient [AA] or
771 elevated O_3 [eO_3]). Each value is the mean ± standard error (n=6).
772 **Figure 3.** Relationships between (A) light-saturated net photosynthetic rate [P_{Nsat}]
773 and stomatal conductance for water vapor [G_{sH2O}], (B) P_N and mesophyll
774 conductance to CO_2 [G_m], (C) P_N and total conductance to CO_2 [G_{totCO2}], (D) G_m
775 and G_{sH2O}, in Siebold's beech. Linear regression analysis was used to assess the
776 significance of the relationship in ambient (AA) and elevated O_3 (eO_3). * P<0.05,
777 *** P<0.001, ns denotes not significant.
778 **Figure 4.** Relationships between leaf gas exchange parameters (light-saturated net
779 photosynthetic rate [P_{Nsat}], stomatal conductance [G_{sH2O}], mesophyll conductance

780 [G_m] and total conductance to CO_2 [G_{totCO2}]) and leaf density (LD) of Siebold's
781 beech saplings under different O_3 concentrations (ambient [AA] or elevated O_3
782 [eO_3]). Simple linear regression analysis was applied to assess the relationships. *
783 $P<0.05$, ns denotes not significant.

784 **Figure 5.** Principal component analysis of parameters derived from analyses of the
785 photosynthetic capacity (P_N/C_c curves), light harvesting (P_N/PPFD curves) and
786 diffusive limitations to CO_2 transport (G_{sCO2}, G_m and G_{totCO2}) of Siebold's beech
787 grown under different O_3 concentrations (ambient [AA] or elevated O_3 [eO_3]).
788 Ellipses represent 95% confidence intervals for measurements conducted in June,
789 August and October. The correlation circle is also shown. Measurements of AA-
790 treated plants in June and August and eO_3-treated plants in June occupy the same
791 position in multi-variate space. On the other hand, eO_3-treated plants analysed in
792 October occupy statistically distinct multi-variate space. Component 1 accounts
793 for 49.2% of the variance within the dataset and component 2 accounts for 14.8%
794 of variance.

795

796

797

798

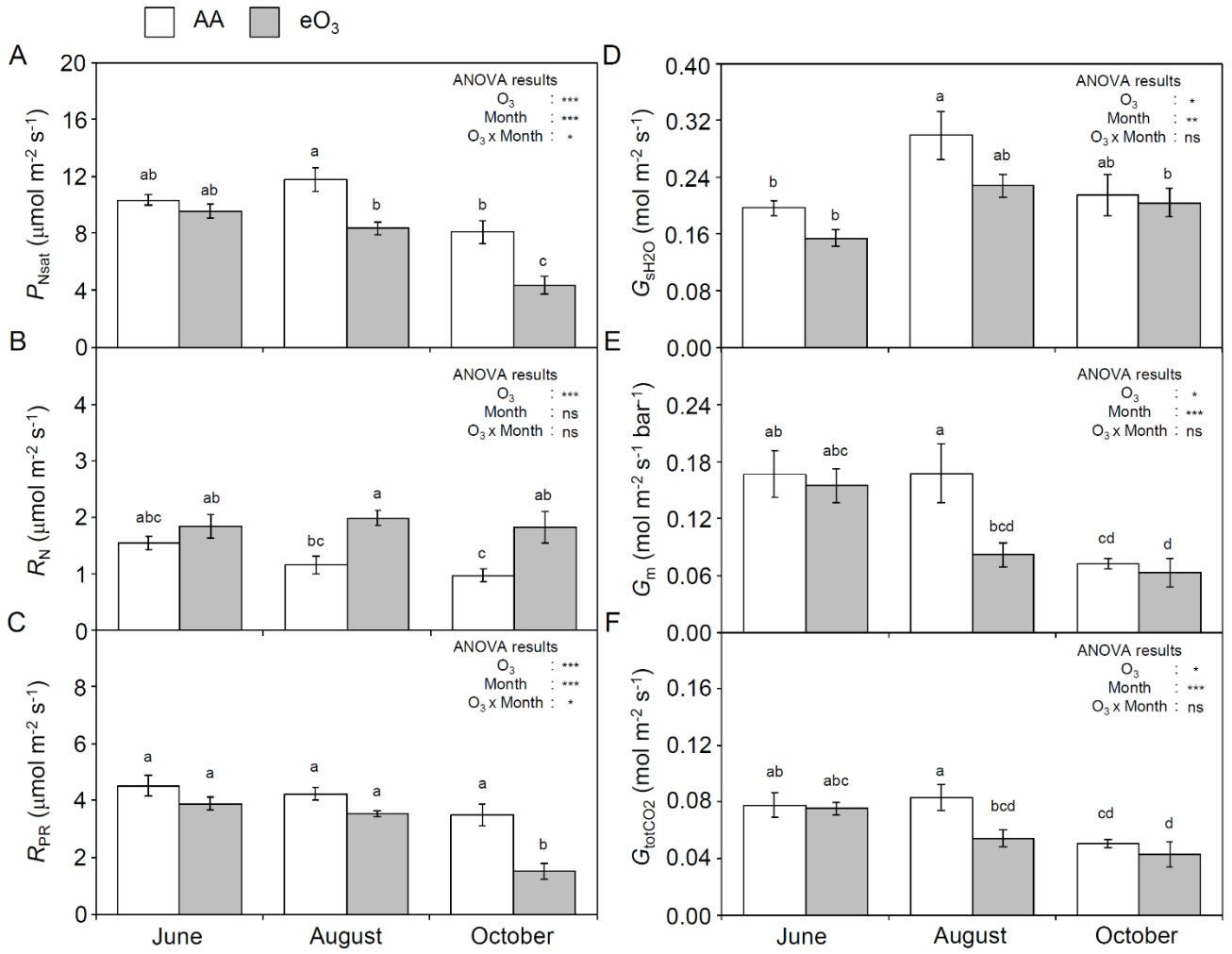

Figure 1. Photosynthetic parameters of Siebold's beech grown under ambient (AA) and elevated O_3 (eO_3): (A) Light-saturated net photosynthetic rate [P_{Nsat}], (B) dark respiration rate [R_N], (C) photorespiration [R_{PR}], (D) stomatal conductance to water vapor [G_{sH2O}], (E) mesophyll conductance to CO_2 [G_m], (F) total conductance to CO_2 [G_{totCO2}]. Each value is the mean ± standard error (n = 6). Two-way ANOVA: * p<0.05, ** p<0.01, *** p<0.001, ns denotes not significant. Different letters show significant differences among treatments (p<0.05, Tukey test).

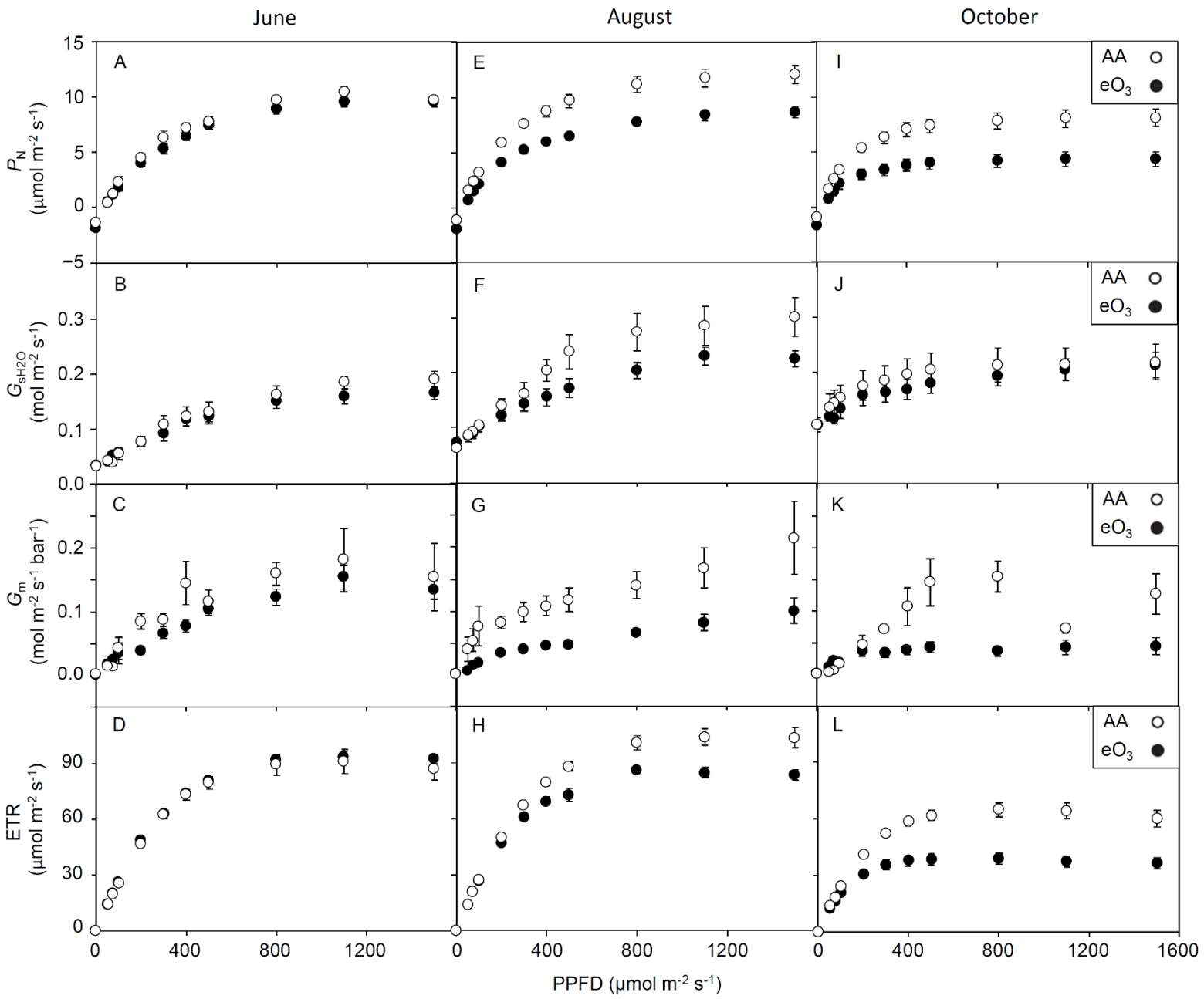

Figure 2. Responses of net photosynthetic rate (P_N), stomatal conductance (G_{sH2O}), mesophyll conductance (G_m) and electron transport rate (ETR) to

photosynthetic photon flux density (PPFD). The P_N/PPFD curves were obtained by measuring P_N over 11 PPFD steps (1500, 1100, 800, 500, 400, 300, 200, 100, 75, 50, 0 μmol m^{-2} s^{-1}) in Siebold's beech exposed to different O_3 concentrations (ambient [AA] or elevated O_3 [eO_3]). Each value is the mean ± standard error (n = 6).

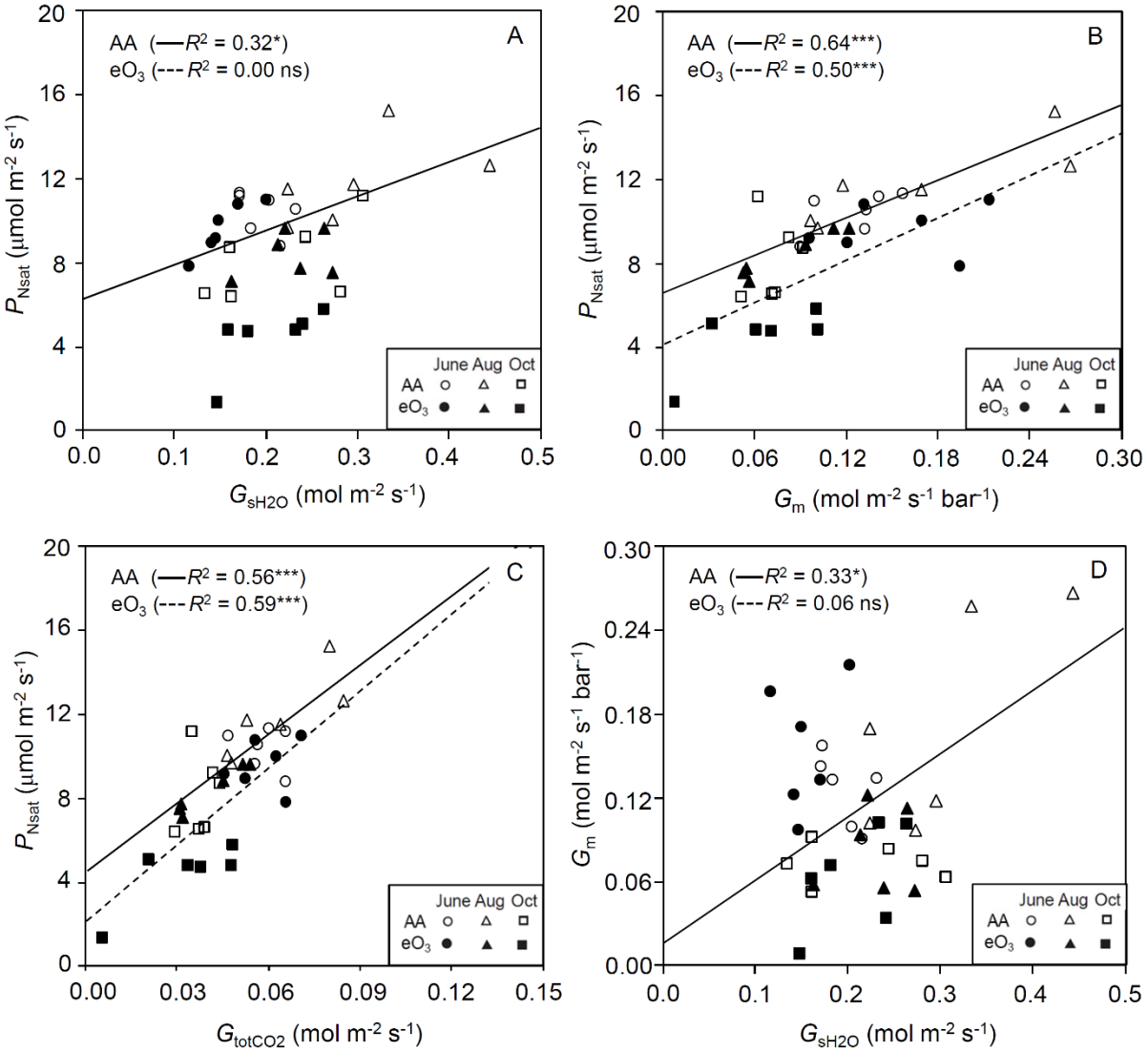

Figure 3. Relationships between (A) light-saturated net photosynthetic rate [P_{Nsat}] and stomatal conductance for water vapor [G_{sH2O}], (B) P_N and mesophyll conductance to CO_2 [G_m], (C) P_N and total conductance to CO_2 [G_{totCO2}], (D) G_m and G_{sH2O}, in Siebold's beech. Linear regression analysis was used to assess

the significance of the relationship in ambient (AA) and elevated O_3 (eO_3). * $p<0.05$, *** $p<0.001$, ns denotes not significant.

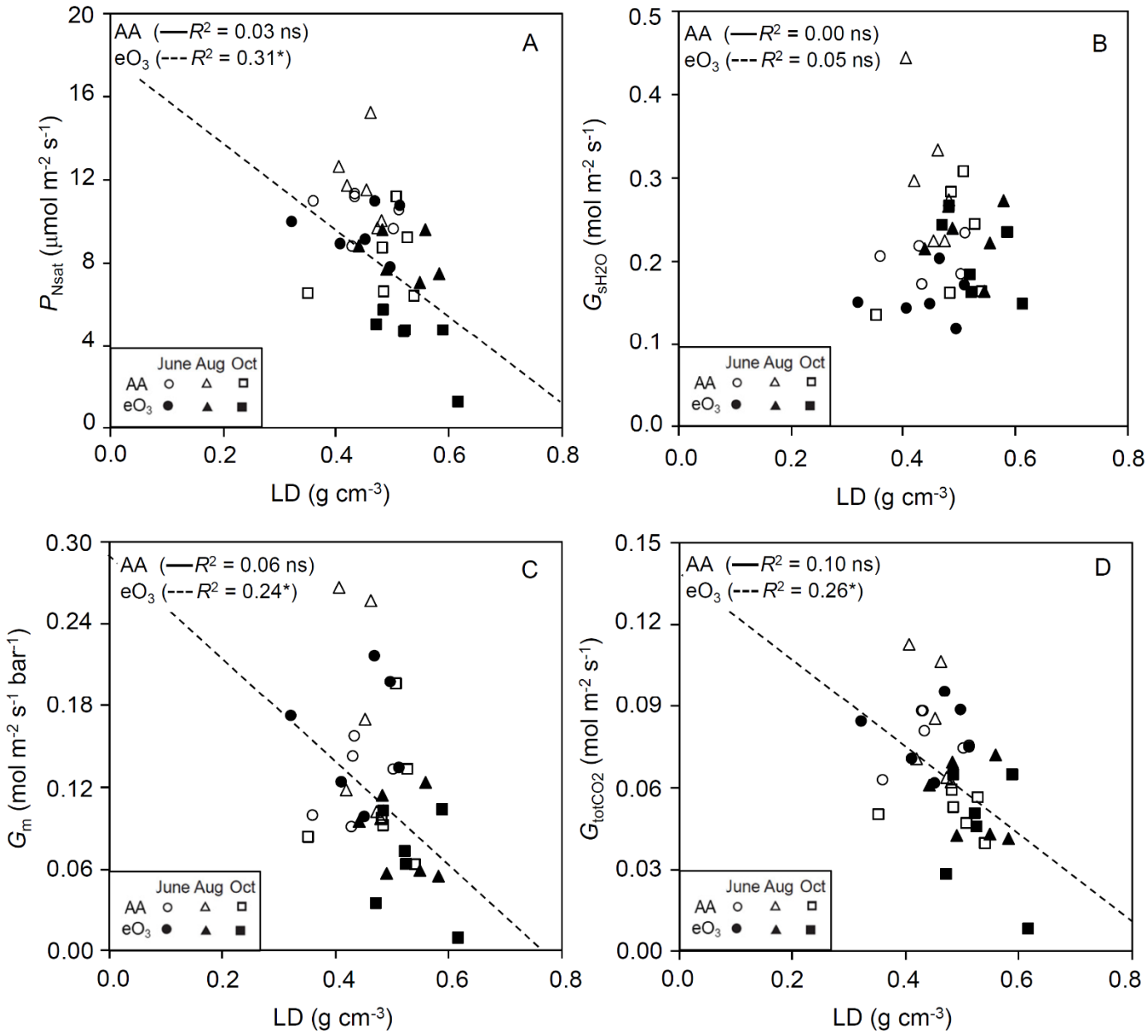

Figure 4. Relationships between leaf gas exchange parameters (A: light-saturated net photosynthetic rate [P_{Nsat}], B: stomatal conductance [G_{sH2O}], C: mesophyll

conductance [G_m] and D: total conductance to CO_2 [G_{totCO2}]) and leaf density (LD) of Siebold's beech saplings under different O_3 concentrations (ambient [AA] or elevated O_3 [eO_3]). Simple linear regression analysis was applied to assess the relationships. * $p<0.05$, ns denotes not significant.

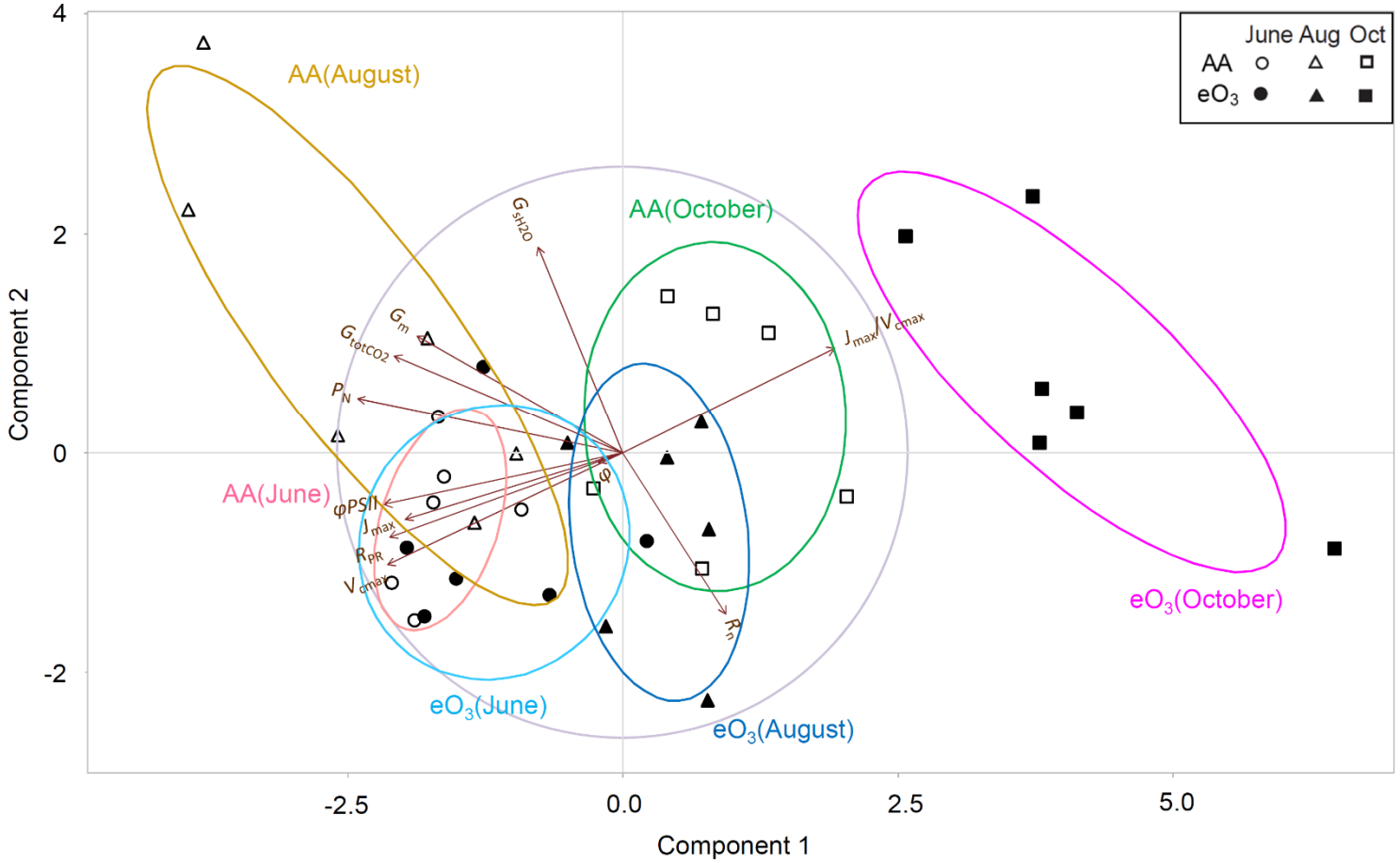

Figure 5. Principal component analysis of parameters derived from analyses of the photosynthetic capacity (P_N/C_c curves), light harvesting (P_N/PPFD curves) and diffusive limitations to CO_2 transport (G_{sCO2}, G_m and G_{totCO2}) of Siebold's beech grown under different O_3 concentrations (ambient [AA] or elevated O_3 [eO_3]). Ellipses represent 95% confidence intervals for measurements conducted in June, August and October. The correlation circle is also shown. Measurements of AA-treated plants in June and August and eO_3-treated plants in June occupy the same position in multi-variate space. On the other hand, eO_3-treated plants analysed in October occupy statistically distinct multi-variate space. Component 1 accounts for 49.2% of the variance within the dataset and

component 2 accounts for 14.8% of variance.

Table 1 Leaf mass per area (LMA), leaf density (LD) and leaf thickness (LT) of Siebold's beech saplings grown under ambient (AA) and elevated O_3 (eO_3) measured in 2012. Each value is the mean ± standard error (n = 6). Two-way ANOVA: * $p<0.05$, ns denotes not significant. Different letters show significant differences among treatments ($p<0.05$, Tukey test).

	LMA (g m^{-2})				LD (g cm^{-3})				LT (mm)			
	AA		eO_3		AA		eO_3		AA		eO_3	
June	90.9 ± 7.3	a	83.0 ± 6.0	a	0.45 ± 0.02	ab	0.44 ± 0.03	a	0.20 ± 0.01	a	0.19 ± 0.01	a
August	81.3 ± 3.0	a	92.0 ± 2.6	a	0.45 ± 0.01	ab	0.52 ± 0.02	bc	0.18 ± 0.01	a	0.18 ± 0.00	a
October	90.8 ± 8.0	a	96.6 ± 4.4	a	0.48 ± 0.03	abc	0.54 ± 0.02	c	0.19 ± 0.01	a	0.18 ± 0.00	a
ANOVA results												
O_3		ns				*				ns		
Month		ns				*				ns		
O_3 × Month		ns				ns				ns		

Table 2 Parameters derived from analyses of light harvesting (P_N/PPFD curves: initial slope of photosynthetic light response curve [Φ], quantum yield of photosystem II photochemistry [φPSII], electron transport rate [ETR]) and photosynthetic capacity (P_N/Cc curve: maximum rate of carboxylation [V_{cmax}], maximum rate of electron transport for RuBP regeneration [J_{max}], the ratio of J_{max} to V_{cmax} [J_{max}/V_{cmax} ratio]) of Siebold's beech grown under ambient (AA) and elevated O_3 (eO_3). Each value is the mean ± standard error (n = 6). Two-way ANOVA: * $p<0.05$, ** $p<0.01$, *** $p<0.001$, ns denotes not significant. Different letters show significant differences among treatments ($p<0.05$, Tukey test).

	Φ (mol mol^{-1})				φPSII				ETR (μmol m^{-2} s^{-1})			
	AA		eO_3		AA		eO_3		AA		eO_3	
June	0.042 ± 0.003	a	0.037 ± 0.002	a	0.20 ± 0.01	ab	0.20 ± 0.01	ab	91.0 ± 6.0	ab	93.4 ± 3.2	ab
August	0.043 ± 0.002	a	0.041 ± 0.001	a	0.22 ± 0.01	a	0.18 ± 0.01	b	103.8 ± 4.6	a	84.8 ± 2.7	b
October	0.044 ± 0.001	a	0.038 ± 0.004	a	0.14 ± 0.01	c	0.08 ± 0.01	d	64.3 ± 4.0	c	37.6 ± 2.9	d
ANOVA results												
O_3		ns				***				***		
Month		ns				***				***		
O_3 × Month		ns				**				**		

	V_{cmax} (μmol m^{-2} s^{-1})				J_{max} (μmol m^{-2} s^{-1})				J_{max}/V_{cmax} ratio			
	AA		eO_3		AA		eO_3		AA		eO_3	
June	66.8 ± 6.9	a	62.7 ± 6.1	a	118.0 ± 7.8	ab	114.9 ± 10.1	ab	1.8 ± 0.1	a	1.9 ± 0.1	a
August	63.2 ± 2.5	a	54.5 ± 6.0	a	113.5 ± 1.8	ab	87.9 ± 6.4	bc	1.8 ± 0.1	a	1.7 ± 0.2	a
October	47.2 ± 4.9	a	24.8 ± 2.4	b	95.2 ± 3.4	abc	70.1 ± 6.1	c	2.1 ± 0.2	a	2.9 ± 0.1	b
ANOVA results												
O_3		**				**				*		
Month		***				***				***		
O_3 × Month		ns				ns				**		

Table 3 Relative contribution of stomatal, mesophyll conductance and biochemical limitations (l_s, l_m and l_b, respectively) to light-saturated net photosynthesis (P_{Nsat}) of Siebold's beech grown under ambient (AA) and elevated O_3 (eO_3). Each value is the mean ± standard error (n = 6). Two-way ANOVA: * $p<0.05$, ** $p<0.01$, *** $p<0.001$, ns denotes not significant. Different letters show significant differences among treatments ($p<0.05$, Tukey test).

	l_s (%)				l_m (%)				l_b (%)			
	AA		eO_3		AA		eO_3		AA		eO_3	
June	27.9 ± 0.8	ab	35.1 ± 2.1	a	35.2 ± 4.7	a	29.6 ± 4.4	a	36.9 ± 5.1	ab	35.3 ± 2.9	a
August	23.9 ± 1.4	b	21.3 ± 1.4	bc	27.2 ± 4.1	a	34.1 ± 4.0	a	48.9 ± 4.9	ab	44.6 ± 4.9	ab
October	22.2 ± 2.7	bc	16.0 ± 1.8	c	36.3 ± 3.2	a	30.3 ± 4.8	a	41.5 ± 2.3	ab	53.7 ± 4.9	b
ANOVA results												
O_3		ns				ns				ns		
Month		***				ns				*		
O_3 × Month		**				ns				ns		

Supplementary materials

Interactive effect of leaf age and ozone on mesophyll conductance in Siebold's beech

Yasutomo Hoshika[1*], Matthew Haworth[2], Makoto Watanabe[3] and Takayoshi Koike[4]

1. Institute of Research on Terrestrial Ecosystems (IRET), National Research Council of Italy (CNR), Via Madonna del Piano, I-50019 Sesto Fiorentino, Italy

2. Institute of Sustainable Plant Protection (IPSP), National Research Council of Italy (CNR), Via Madonna del Piano, I-50019 Sesto Fiorentino, Italy

3. Institute of Agriculture, Tokyo University of Agriculture and Technology, Fuchu 183-8509, Japan

4. Research Faculty of Agriculture, Hokkaido University, Sapporo 060-8689, Japan

*Corresponding author:

Yasutomo Hoshika, Tel: +39-055-522-5949, Fax: +39-055-522-5920

E-mail: yasutomo.hoshika@cnr.it

Supplementary figures

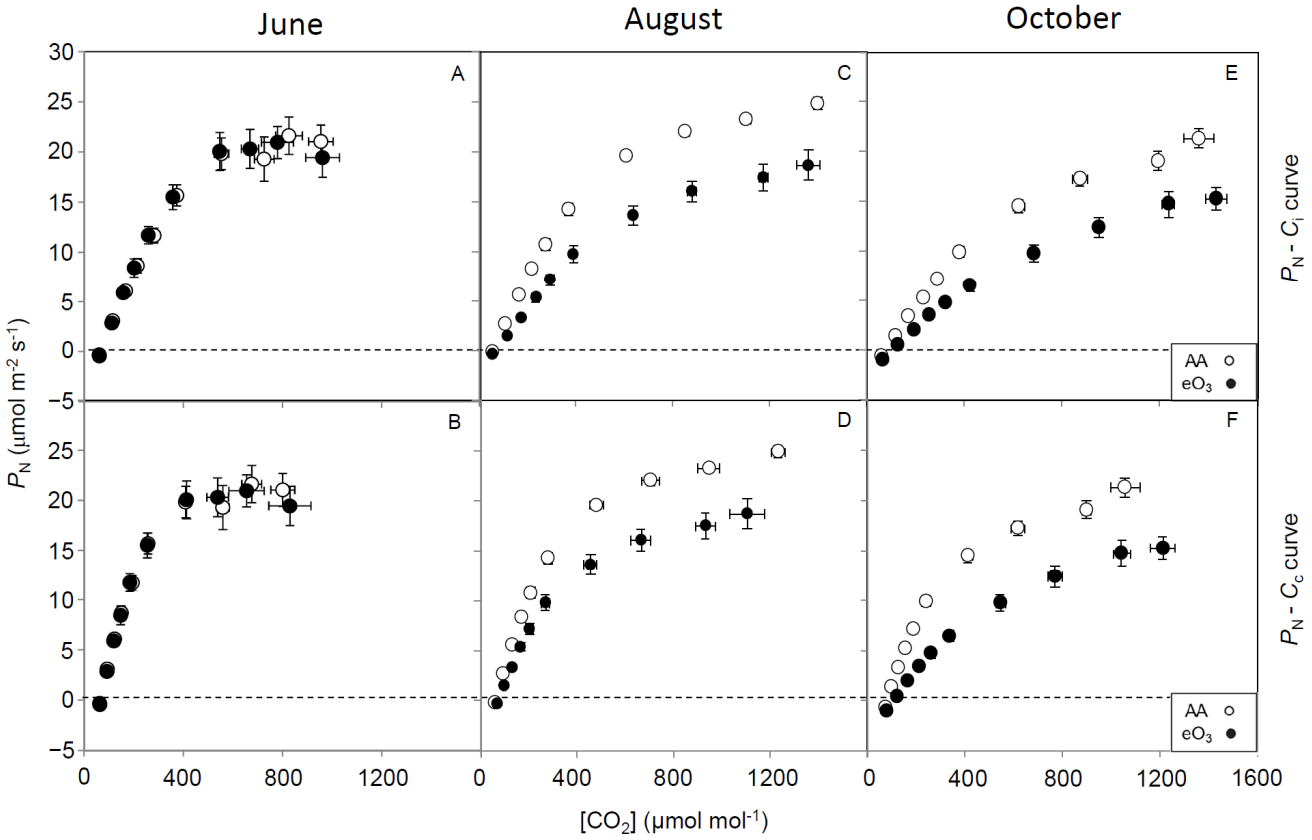

Figure S1. Responses of net photosynthetic rate (P_N) to the sub-stomatal concentration of CO_2 (C_i) (upper figures) or the concentration of CO_2 inside the chloroplast envelope (C_c) (bottom figures) at different ages. The P_N/C_i curves were obtained by measuring P_N over 12 ambient CO_2 concentration steps (C_a, 380, 300, 220, 140, 60, 300, 380, 500, 800, 1100, 1400, 1700 µmol mol^{-1}). Values of G_m derived from the curve fitting method (Ethier and Livingston, 2004) were used to calculate the P_N/C_c curves. Each value is the mean ± standard error (n = 6).

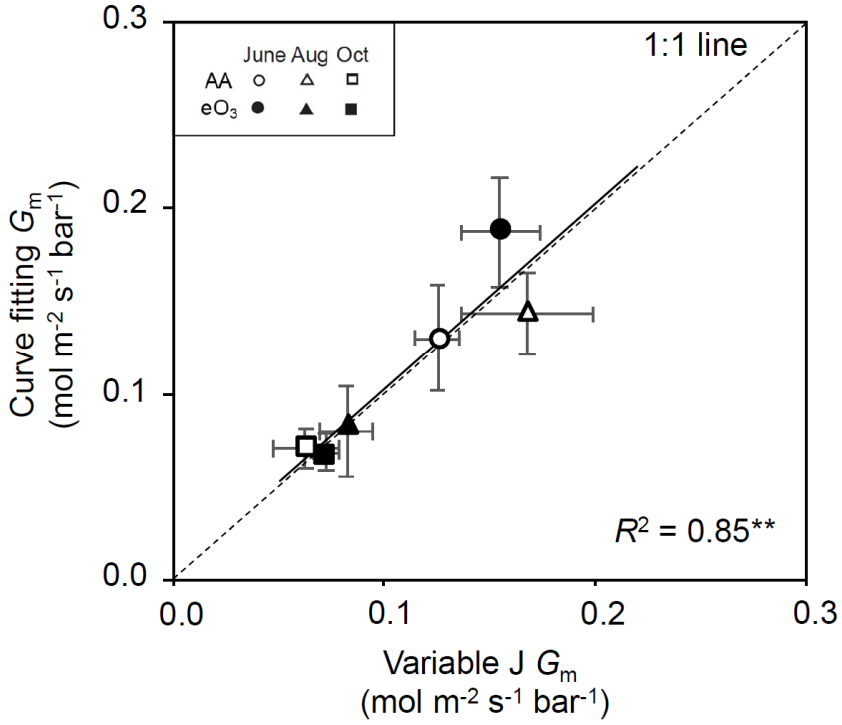

Figure S2. Relationship between mesophyll conductance (G_m) values derived from the variable J method and those derived from the P_N/C_i curve fitting method in Siebold's beech exposed to different O_3 concentrations (ambient [AA] or elevated O_3 [eO_3]). Each value is the mean ± standard error (n = 6). A linear regression analysis: ** p<0.01.

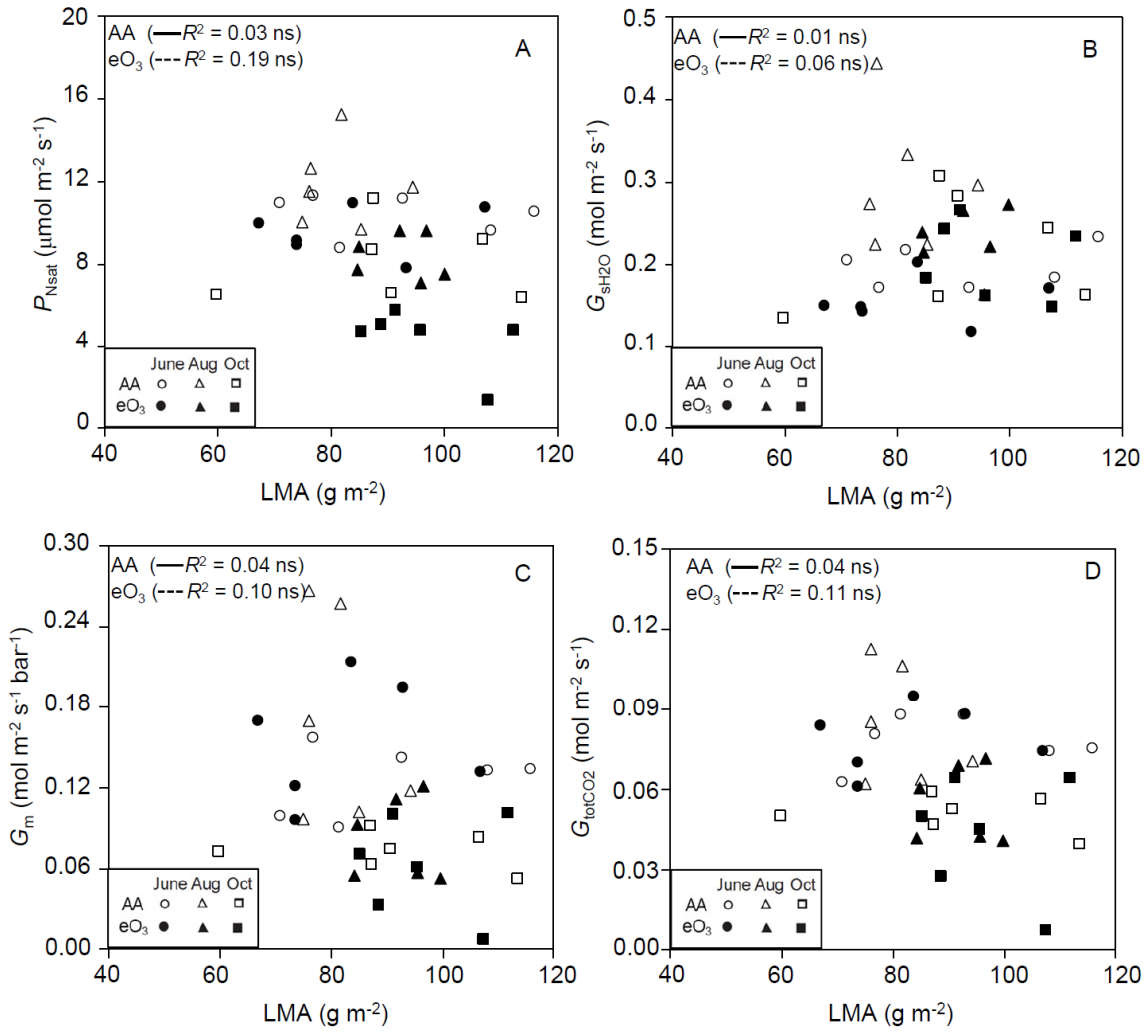

Figure S3. Relationships between leaf gas exchange parameters (A: light-saturated net photosynthetic rate [P_{Nsat}], B: stomatal conductance [G_{sH2O}], C: mesophyll conductance [G_m] and D: total conductance to CO_2 [G_{totCO2}]) and leaf mass per area (LMA) of Siebold's beech saplings under different O_3 concentrations (ambient [AA] or elevated O_3 [eO_3]). Simple linear regression analysis was applied to assess the relationships. ns denotes not significant.

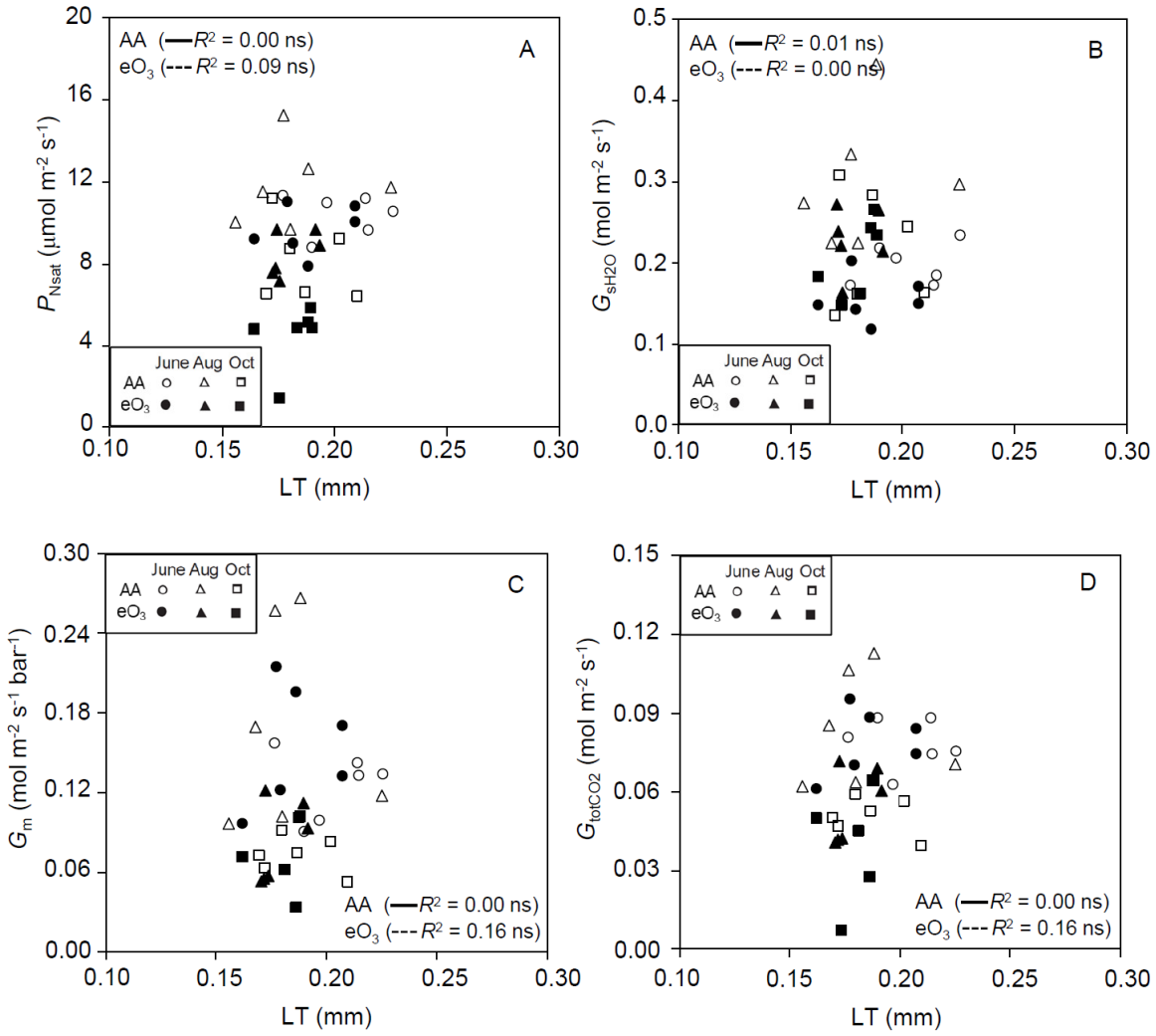

Figure S4. Relationships between leaf gas exchange parameters (A: light-saturated net photosynthetic rate [P_{Nsat}], B: stomatal conductance [G_{sH2O}], C: mesophyll conductance [G_m] and D: total conductance to CO_2 [G_{totCO2}]) and leaf thickness (LT) of Siebold's beech saplings under different O_3 concentrations (ambient [AA] or elevated O_3 [eO$_3$]). Simple linear regression analysis was applied to assess the relationships. ns denotes not significant.